Hindawi Publishing Corporation
International Journal of Antennas and Propagation
Volume 2016, Article ID 8782671, 8 pages
http://dx.doi.org/10.1155/2016/8782671

Research Article

Investigation of Shadowing Effects in Typical Propagation Scenarios for High-Speed Railway at 2350 MHz

Liu Liu,[1,2,3] Cheng Tao,[1,3] David W. Matolak,[2] Tao Zhou,[1] and Houjin Chen[1]

[1]*Institute of Broadband Wireless Mobile Communications, Beijing Jiaotong University, Beijing 100044, China*
[2]*Department of Electrical Engineering, University of South Carolina, Columbia, SC 29208, USA*
[3]*National Mobile Communications Research Laboratory, Southeast University, Nanjing 210096, China*

Correspondence should be addressed to Liu Liu; liuliu@bjtu.edu.cn

Received 18 May 2016; Accepted 25 September 2016

Academic Editor: Tamer S. Ibrahim

Based on realistic measurements in China, shadowing characteristics at the frequency of 2350 MHz were investigated in typical High-Speed Railway environments. After confirming that the measured shadowing satisfies wide-sense stationarity (assessed via the reverse arrangement test method), we quantify the shadowing correlation. Three types of correlation models are compared for the shadowing characterization, and the Normalized Mean Square Error is used to determine the best matching model: a single decaying exponential function. Decorrelation distances were found to be 11.9 m, 17.7 m, and 8.3 m in our three HSR scenarios, respectively. The results should be useful for the evaluation and verification of wireless communication in High-Speed Railway scenarios.

1. Introduction

It is becoming increasingly apparent that providing broadband wireless communications to high-speed trains is a particularly important and challenging task. Passengers and railway operators are eager for higher data rates and more reliable wireless communications between the train and trackside networks, independent of their locations or speeds.

For the design and performance evaluation of wireless communication systems in High-Speed Railway (HSR) scenarios, it is of crucial importance to have accurate and realistic propagation channel models between the train and ground stations. Shadow fading is the large-scale fluctuation of the signal envelope due to large (with respect to a wavelength) objects obstructing the propagation paths between the transmitter and the receiver. The shadowing obstacle absorbs and/or blocks the transmitted signal and determines the relatively slow signal variations with respect to the nominal value given by path loss models. Hence the shadowing characterization results are usually used to adjust link budget path loss calculations for statistical coverage estimates in wireless network planning. An effect analogous to obstruction can also be observed in some channels with a line-of-sight (LOS) component, in which multiple reflections can induce relatively slow variation (in addition to the more rapid small-scale fading).

Previous work shows that the shadowing effect significantly affects handover behavior, intra- and inter-cell interference, and the diversity performance. For the HSR propagation environment, the shadowing effect is of primary importance for wireless network planning. To date, there has been increasing published literature on this research topic. Several shadowing models for open terrain settings have been proposed [1–5]. Several shadowing models are characterized by the independent log-normal random variable, from sample to sample. Due to the nature of the propagation environment, the shadowing effect for a radio link over some range of locations will not change significantly: the shadowing samples are in fact correlated. In [6], a spatial correlation model was established for cellular settings using an exponential function; shadowing correlation decreases as the receiver moves. Another kind of correlated shadowing

model considering the angular direction is very useful to characterize the correlation between two links that involve a single receiver and two base stations, for example, [7, 8] by Graziosi. The effects of correlation of shadow fading affect the links between the mobile terminal and the various base stations, which are important to determine interference statistics and to drive handover operations in cellular networks. Taking this correlation into account, the researchers used the exponential function to characterize the shadowing effect for the open hilly HSR terrain [9]. In the published results, when extracting the autocorrelation properties of shadowing samples, researchers used the basic definition of the correlation, as expressed in equation (6) in [10]. The correlated samples, equally spaced by distance Δd, may be gathered from one measurement run. In order to gather reliable statistics, these experimental data should be statistically stationary. However, previous research simply assumed that the experimental shadowing data is stationary.

In this paper, we analyze the characteristics of the shadowing effect in typical HSR environments. After extracting the statistical properties of the shadowing effect, we employ a reverse arrangement test to verify the wide-sense stationarity (WSS) of shadowing records. Based on the verification of stationarity, we can (i) set any geographical point between the transmitter and receiver as the starting position for correlation estimation and (ii) extract the channel parameters from one measurement run rather than the ensemble averaging the samples from multiple measurements in homogeneous propagation environments. Then we compare three correlation models for the shadowing characterization, and the Normalized Mean Square Error (NMSE) is used to determine the best fitting model.

The rest of this paper is organized as follows. In Section 2 we describe the measurement campaigns and work sites. In Section 3, path loss models including the path loss exponent and statistical properties of shadowing effects are extracted using the least square estimation method. In Section 4, the stationarity of shadowing samples using the reverse arrangement method is demonstrated, and then three types of correlation models are fit to the measurement data. The conclusions are drawn in Section 5.

2. Measurement Descriptions

The radio environments of interest were probed with the well-accepted wideband channel sounder Propsound developed by Elektrobit. The transmitter uses a loadable rectangular chip sequence as the excitation signal. At the receiver, the channel impulse response (CIR) is obtained by a sliding correlator that correlates the received wave with a copy of the transmitter sequence. The measurement parameters are listed in Table 1. GPS receivers were used at both the transmitter and receiver for distance determination and synchronization.

Typical HSR terrains, the open viaduct (OV) and tree-blocked viaduct (TBV), which can incur the seasonal effects, and the open railway cutting (ORC) environments are considered in this paper. The viaduct is a long bridge-like concrete structure, built over the ground with height of approximately 10 m–20 m. The viaduct is one of the most common environments in HSR (occupying 80% of the entire HSR, both in operation and under construction). The railway cutting is a specific construction of railway with sloped sidewalls, where soil or rock material from a hill or mountain is cut out to make way for a railway line.

Table 1: Channel measurement campaigns on HSR.

Item	Value
BT channel measurement [2]	
Central frequency	2350 MHz
Snapshot rate	984 Hz
Bandwidth	10 MHz
Velocity	240 km/h
m sequence length	127
Power (OV)	37 dBm
ZX channel measurement	
Central frequency	2350 MHz
Snapshot rate	1986.5 Hz
Bandwidth	50 MHz
Velocity	200 km/h
m sequence length	127
Power (TBV and ORC)	(30.8, 32.7) dBm

In this paper, the OV experimental data was gathered from the measurement conducted on the Beijing-Tianjin (BT) HSR. The propagation environment was open and clear. It was composed of the viaduct and roadbed and covered with agricultural fields. No obstruction could be observed in the signal path. Technically, with no obstruction of the LOS component, the physical effect is not actually shadowing, but rather the large-scale variation of power due to multipath components whose effect can be analyzed analogously to the actual obstruction case. This measurement was performed in winter, 2011. For brevity, we do not include extensive details here; more detailed description can be found in [2]. In LOS propagation environment, the variation of path loss is caused (almost surely) by other multipath components (generally we would call this small-scale effects). The variation of path loss in LOS settings is an inherent characteristic of the way we model path loss. If the distance dependent component of path loss is removed, in LOS settings, what remains must be the multipath. For some geometries, this multipath (e.g., surface reflection) can indeed vary slowly, hence taking on the appearance of a large-scale effect.

The measurement data from the TBV and ORC environments are obtained from the measurement campaigns conducted on Zhengzhou-Xi'an (ZX) HSR in summer, 2012. The propagation sites are shown in Figures 1 and 2, respectively. In the measurement runs, the receiver equipment was positioned on a test train. A carriage-roof mounted antenna was directly linked to the receiver to avoid the penetration loss from the metal train body.

In the TBV terrain, the transmitter and rail-track were separated by a distance of 92 m. The transmitter antenna was raised approximately 5 m high by a lift tower. This tower

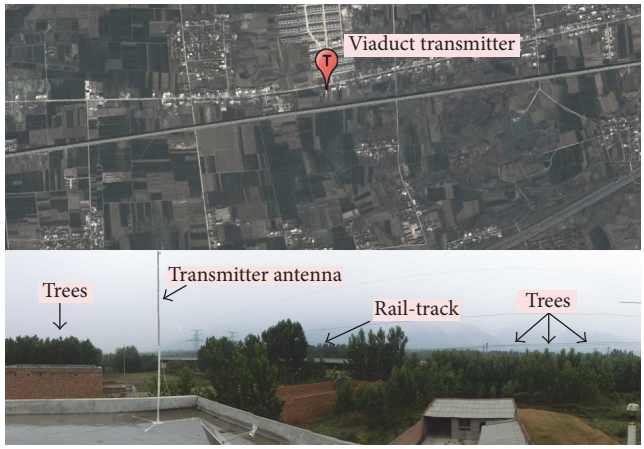

Figure 1: Propagation condition of the TVB on ZX HSR.

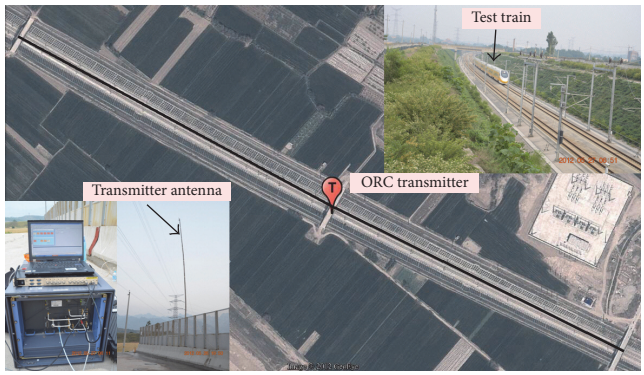

Figure 2: Propagation condition of the ORC on ZX HSR.

was located on the roof of a two-floor building with the height of 8 m which yielded the same height as the viaduct nearby. The transmitter (Tx) antenna was thus at a height above ground of 13 m. Trees obstructed a significant portion of the propagation path. During the days in or around summer, thick trees around the rail will block the train-ground propagation link, causing deeper signal variation. This terrain is considered as the non-line-of-sight (NLOS) scenario and is the main difference between the OV and TBV environments. In the ORC scenario, the transmitter antenna was placed on an overbridge across the RC and raised approximately 8.8 m. The measured cutting was near the HuaShan North Station, with a depth of about 5 m and a length of 2000 m. There are no obstacles in the signal path, which makes the RC scenario another typical LOS propagation scenario.

3. Shadowing Fading Characterization

To investigate the shadowing effect, the power attenuation, namely, path loss, needs to be extracted first. Commonly, the received power attenuation depends on the distance between the transmitter and the receiver. Here the received signal power at the time index t_{av}, which corresponds to the set of geographical measurement positions, can be calculated as

$$P_{Rx}\left(it_{\mathrm{av}}\right) = \frac{1}{W}\sum_{n=iW}^{(i+1)W-1}\sum_{l=0}^{L-1}\left|h\left(nt_{\mathrm{rep}}, l\Delta\tau\right)\right|^2, \tag{1}$$

where t_{rep} stands for the snapshot repetition rate, L is the number of the discrete multipath components, $\Delta\tau$ denotes the time delay resolution, $h(nt_{\mathrm{rep}}, l\Delta\tau)$ represents the CIR at the t_{rep} repetition sample instant, and W is the width of the averaging window over which the small-scale fading effect (multipath component and Doppler shift) can be removed. Here twenty wavelengths (2.6 m) yields at a relative speed of 200 km/h an averaging time interval of $t_{\mathrm{av}} = 47$ ms, that is, $W = 40$ snapshots. After obtaining the received power versus the distance between the transmitter and the receiver, the empirical path loss model in decibels can be used for the power attenuation prediction as

$$\mathrm{PL}\,(d) = A + 10 \cdot n \cdot \log 10\,(d) + X_{\sigma}, \tag{2}$$

where d is the link distance in meters, n is the path loss exponent, A is the intercept, and X_{σ} represents the shadowing term. In the measurement data processing, the linear regression based on Least Squares is employed to estimate A and n. Since the shadowing introduces additional power fluctuations and causes the received local-mean power to vary around the area-mean, the shadowing samples are obtained by subtracting the least-squares interpolated loss model values (2) from the actual measurement data found via (1). When employing the most commonly used log-normal process for the characterization of shadowing, the shadow fading process can be parameterized as a set of zero-mean Gaussian random variables with different standard deviation values as

$$X_{\mathrm{OV}} \sim \left(0, 2.0^2\right), \quad d > 80, \tag{3}$$

see [2]

$$\begin{aligned} X_{\mathrm{TBV}} &\sim \left(0, 2.51^2\right), \quad d > 90, \\ X_{\mathrm{ORC}} &\sim \left(0, 1.86^2\right), \quad d > 40, \end{aligned} \tag{4}$$

where X_{TBV} and X_{ORC} are computed by using the experimental data from the ZX HSR.

It is obvious that the standard deviation value of the open terrain is smaller than that in the tree-blocked terrain. This result is identical with the previous empirical studies which suggest that X_{σ} should increase with the density of obstructions and scatterers. In the open environment the variation of the signal strength is attributed to the changes in reflecting surfaces and scattering objects. It is is an inherent characteristic of the way we model path loss. When the surface reflection varies slowly, as noted, this can take on the appearance of a large-scale effect. Furthermore, the standard deviation for the ORC scenario is less than the value in the OV environment. This is because the Tx-to-Rx link distance of the ORC environment is smaller than the OV model. The

average attenuation of X_σ from reflection objects increases with the distance due to the potential for a larger number of attenuating objects at larger distance. Therefore, the signal variation in ORC is smaller than the result in OV.

4. Validation of Stationary Shadowing Samples

4.1. Motivation. When characterizing the shadowing effect, which is considered a random process, the properties of this phenomenon can be hypothetically characterized at any time instant by computing average values over the sample collection that describes the random process. In most previous research, the experimental shadowing data is simply assumed stationary.

(1) Ensemble Average. For the general case where the mean value (first moment) and the correlation value (second moment) of the random process do not vary with the observation time t, the random process is said to be wide-sense stationary. Contrarily, the properties of a nonstationary random process are generally time-varying functions. The functions can only be determined by performing averages over the ensemble of sample functions forming the process. A good estimate of the autocorrelation coefficient in data processing requires ensemble averages (statistical averages) by taking as many samples as possible into account. Ergodicity is typically assumed, and measurements are taken for all possible shadowing samples at each specified geographical position. It is infeasible to obtain very large data sets in HSR channel measurements due to the great expense [11]. Additionally, in published documents, the auto- and cross-correlation properties are calculated by using the assumed definition of the sample correlation, as expressed as equation (6) in [10]. The correlated samples, equally spaced, may be gathered from one measurement run. However, most correlation investigation does not consider the stationarity verification.

(2) Determination of Initial Distance. In [6], Gudmundson proposed an exponential correlation model ((5) discussed in Section 4) to describe the correlated shadowing effect in cellular settings. It is logical that this model is infeasible when simulating the correlated shadowing sequence if WSS does not hold. The reason is that the correlation value at an arbitrary two geographically separated positions may vary from position to position if the shadowing samples are nonstationary. The autocorrelation value in (5) is normalized according to a starting position x_0, and it is position-dependent. However, when simulating nonstationary correlated shadowing sequences, other than via site-specific measurement data, one does not have information on how to select the actual autocorrelation value. For example, let us assume that the mobile terminal begins at the initial transmitter receiver distance x_1 with a speed of v; this initial distance x_1 is independent of the initial separation distance x_0 in the channel characterization model; generally $x_1 > x_0$ ($x_0 = 0$ m in [12]).

If the experimental samples are stationary, two problems are solved. By invoking stationarity, (i) we can use the experimental data from one measurement run for the channel parametrization instead of ensemble averages (statistical averages) by taking all possible samples into account; (ii) we can set any geographical point between the transmitter and receiver as the starting position when simulating the correlated shadowing sequence or characterizing the correlation model.

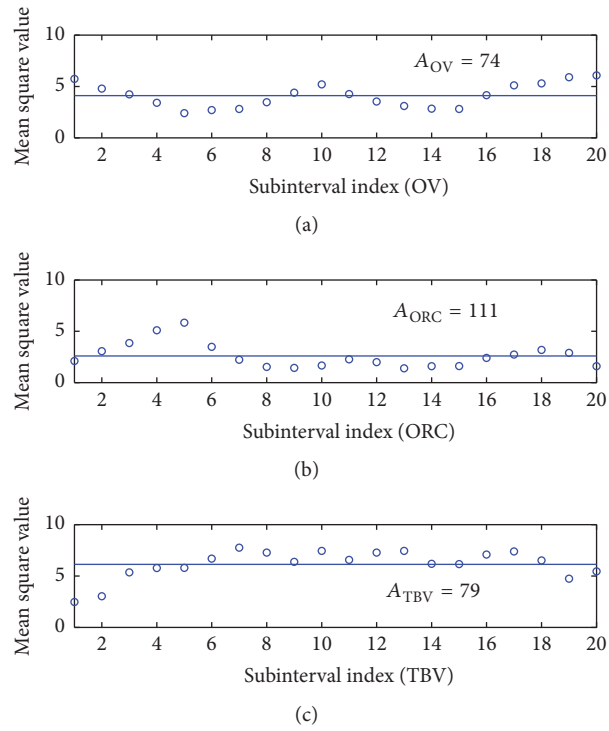

Figure 3: Examination results for WSS shadowing characteristics. The solid blue lines denote the mean values of sequential mean square values. (a) Mean square values of subinterval shadowing samples from the OV environment. (b) Mean square values of subinterval shadowing samples from the ORC. (c) Mean square values of subinterval shadowing samples from the TBV.

4.2. Stationarity Verification Method. In practice, measurement data are often collected under circumstances that do not permit an assumption of stationarity based on simple physical considerations. We use the reverse arrangement (RA) test for testing stationarity. This method does not require knowledge of the sampling distribution. The procedure is described in the Appendix.

By using this method, we divide the overall shadowing sample (Gaussian RVs in the dB scale) records into $N = 20$ equal time intervals and then compute the mean square values within each interval $(x_1^2, x_2^2, x_3^2, \ldots, x_{20}^2)$. Figure 3 shows the 20 subinterval mean square values estimated during the test. It shows that there are small changes, including small positive and negative shifts about the mean value.

From the equation (4.51)–(4.53) in [13], we can get the total number of reverse arrangements $A_{OV} = 74$, $A_{ORC} = 111$, and $A_{TBV} = 79$ from the experimental data of the ORC, OV, and TBV, respectively (see the Appendix for details).

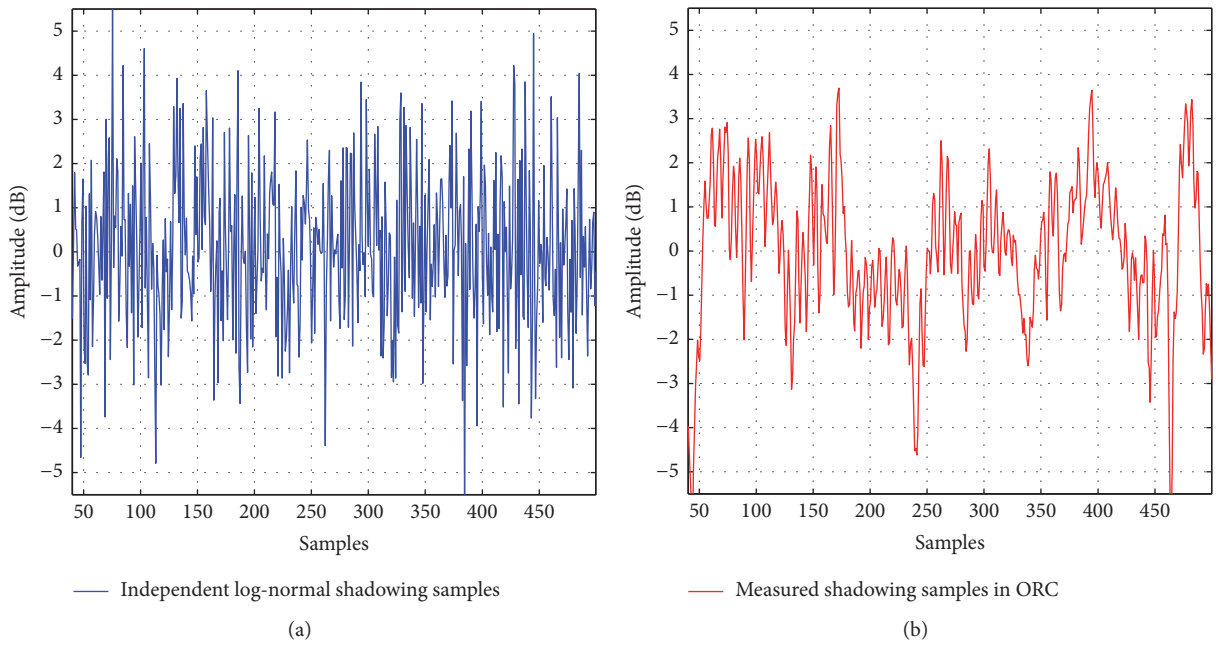

FIGURE 4: Comparisons of the simulated independent sequence and experimental result. The solid blue line denotes the simulated independent shadowing samples obeying the distribution of (3). The solid red line represents the experimental samples from the measurement data in ORC.

Since the obtained reverse arrangements, A_{OV}, A_{ORC}, and A_{TBV} fall within the range between the probabilistic thresholds of 64 and 125, the hypothesis of stationarity is accepted at the 95% significance level, meaning that the shadowing sample data can reasonably be assumed to be WSS. By using this result, we can extract the correlation values corresponding to different intervals from one measurement run.

4.3. Best Fit Autocorrelation Model. Equations (3) and (4) give the distribution parameters of the shadowing recordings. Generally, the high-speed train runs in a wide geometrical space. Due to the nature of the propagation environment, the size or shape of obstructing objects in the signal path, and reflecting surfaces being relatively large, the shadowing effect for the same radio link at the nearby locations will not change significantly. That is to say, the shadowing experienced on nearby propagation paths is related. Figure 4 plots the comparison result of the simulated independent shadowing sequence and the experimental data gathered from the ORC environment. The measured results explicitly show that the neighboring experimental samples appear highly similar and are not independent. For this reason, the autocorrelation function can be applied to characterize the shadowing effect, which can improve the realistic accuracy of propagation models. The correlated model describes the autocorrelation of shadowing decreasing with increasing distance separation. The single correlated negative exponential model proposed by [6] was modified as [12]

$$r_s(d) = e^{-|vt-x_0|/D} = e^{-d/D}, \tag{5}$$

where v denotes the mobile velocity, x_0 refers to the starting distance separation between the transmitter and receiver, and t represents the sampling interval. Thus, $|vt - x_0| = d$ stands for the distance between the current observation position and x_0. D is called the decorrelation distance, which is an area-dependent value. The distance D is taken for the normalized autocorrelation to fall to 0.37 (e^{-1}). Note that the result of the correlated model is the correlation coefficient; that is, this correlated exponential model is normalized.

By using the result from our WSS verification, correlated shadowing results from one measurement run, having the same spatial intervals, can be used for ensemble averages. We denote all the gathered shadowing samples from overall snapshots by a measurement set $S = \{\varepsilon_1, \varepsilon_2, \ldots, \varepsilon_s\}$ and define Δd as the separation distance between two sequential samples. The stationarity property allows us to express the autocorrelation only as the function of the interval of time or space. Thus, by using the time-distance relationship, the autocorrelation coefficient $\rho(\Delta d)$ of shadow fading is estimated over set S_q at a series of discrete distances Δd as

$$\rho(\Delta d) = \frac{\sum_{(i,j)\in\Im_k} (\xi_i - \mu_{k1})(\xi_j - \mu_{k2})}{\sqrt{\sum_{(i,j)\in\Im_k} (\xi_i - \mu_{k1})^2} \cdot \sqrt{\sum_{(i,j)\in\Im_k} (\xi_j - \mu_{k2})^2}}, \tag{6}$$

where $\Im = \{(i,j) : (d_i - d_j) = d;\ \xi_i, \xi_j \in S_q\}$. In (6), μ_1 and μ_2 are the mean values of sets $\{\xi_i : \xi_i \in S;\ i, j \in \Im\}$ and $\{\xi_j : \xi_j \in S;\ i, j \in \Im\}$, respectively.

If observation samples are equally spaced Δd on a straight track line, the exponential form of (5) can be modified to take the form of a stationary model. Then stationary

autocorrelation value of two observation locations with a larger separation distance of $k\Delta d$ satisfies

$$r_m(k\Delta d) = \overbrace{e^{\rho_s} \cdot e^{\rho_s} \cdots e^{\rho_s}}^{k} = e^{k\cdot\rho_s}, \quad (7)$$

where $r_m(\Delta d) = e^{\rho_s}$ denotes the autocorrelation coefficient of the neighboring position spaced by a distance Δd (here we use $\Delta d = 1$ m) and k is a positive integer. Physically speaking, autocorrelation property of the stationary shadowing effect is dependent on the observation separation but independent of the initial position.

For the comparison, two additional correlation models are considered.

(1) The Gaussian Model. This model (also for cellular coverage) was proposed to obtain a definite second derivative of the correlation function at the origin as [14]:

$$r_2(d) = e^{-(1/2)(d/D_c)^2}, \quad (8)$$

where D_c is the modified decorrelation distance.

(2) The Biexponential Model. This model was proposed in [15, 16] for the cellular and mobile satellite channels, respectively, as

$$r_D(d) = ae^{-d/D_1} + (1-a)\,e^{-d/D_2}, \quad (9)$$

where both D_1 and D_2 are tunable parameters. The double exponential decay model provides a better match to the empirical autocorrelation function in certain terrain.

With the nonlinear least-squares estimation method, we can obtain the channel parameters with respect to (3) and (4) for the three areas, OV, TBV, and ORC, respectively. We quantify the "difference" between the extracted model and the measurement data by using NMSE. NMSE is expressed as

$$\text{NMSE} = \frac{\text{norm}\,|r(d) - \tilde{r}(d)|}{\text{norm}\,|r(d)|}, \quad (10)$$

where norm denotes the Euclidean length.

Figure 5 plots the results of the measurement data and the three types of models against the separation distance in the OV, TBV, and ORC cases, respectively. By observation of Table 2 and Figure 5, we can find that Model 1 matches the measured data better than Model 2 and Model 3. Model 3 performs only slightly worse than Model 1 but is more complex, with two parameters instead of one.

Figure 6 provides a comparison between the extracted results and several commonly used cellular channel models against the separation distance between the transmitter and the receiver. It is obvious that, in open environments, that is, OV or ORC environments, the sequential shadowing samples show lower correlation than the result of the TBV environment. This is expected, as we have previously described. The LOS scenario makes the correlated sequential shadowing samples change more rapidly. In TBV, however, the path strength changes less rapidly due to the nearly homogeneous blocking of trees. In Figure 6, proposed exponential models

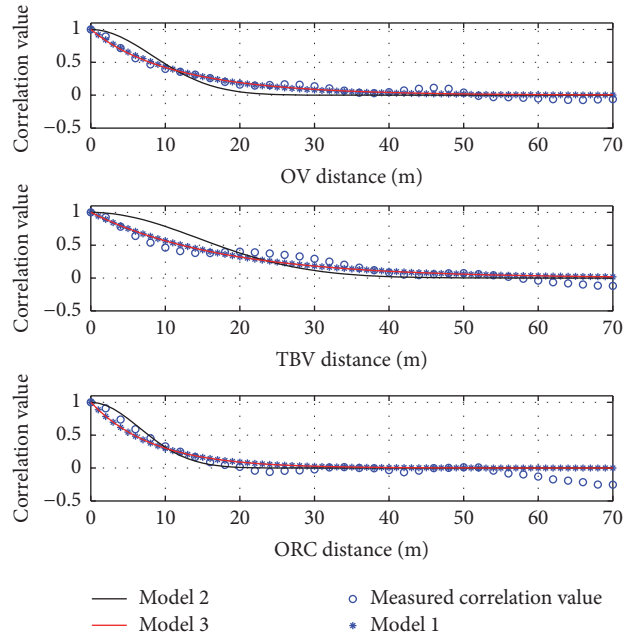

Figure 5: Comparisons of three autocorrelation shadowing models against the raw data.

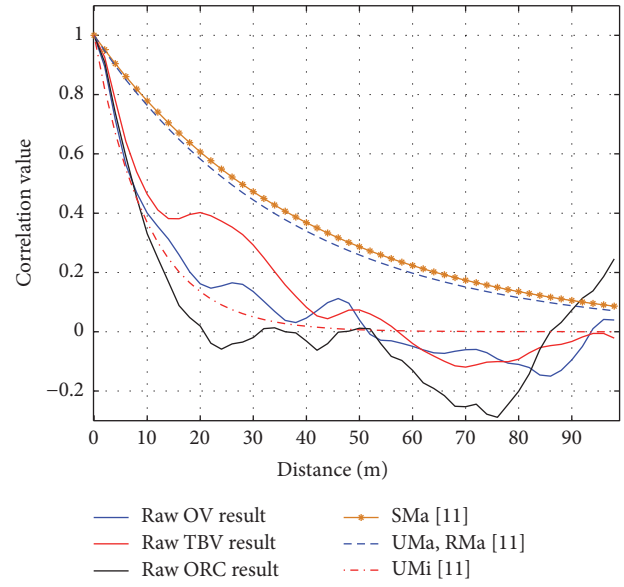

Figure 6: Correlation values against the transceiver separation.

for the cellular system are compared. In [12], decorrelation distances in Suburban Macro (SMa), Urban Macro (UMa), and Rural Micro (RMa) areas are relatively large, approximately 40 m, 37 m, and 37 m, respectively. In Urban Micro (UMi) areas, though, the decorrelation distance decreases to as low as 10 m because the propagation link is fully shadowed by dense concrete buildings. In this figure, it also can be observed that the correlation values in SMa, UMa, and RMa are larger than in open HSR terrains. We hypothesize that the differences are attributable to the following reasons. First, the operating frequency is different. Results of SMa, UMa,

Table 2: Channel measurement campaigns on HSR.

	Model 1: $r_m(k\Delta d) = e^{k\cdot\rho_s},\ \rho_s = -1/D$		Model 2: $r_2(d) = e^{-(1/2)(d/D_c)^2}$	
	Value D	NMSE	Value D_c	NMSE
OV	11.9	0.25	8.2	0.37
TBV	17.7	0.25	14.4	0.41
ORC	8.3	0.40	6.6	0.47
	Model 3: $r_D(d) = ae^{-d/D_1} + (1-a)e^{-d/D_2}$			
	Value a	Value D_1	Value D_2	NMSE
OV	0.86	13.2	5.0	0.27
TBV	0.12	17.7	17.6	0.29
ORC	0.99	8.36	8.36	0.42

and RMa are extracted from the measurements conducted at the frequencies of 900 MHz and 1800 MHz. Generally, radio signals with higher frequency tend to suffer from more power loss of diffraction and reflection. So shadowing correlation effects will be reduced if the frequency is higher. Second, the correlation property in the blocked viaduct case is comparable to that for the UMi case. These lower correlations arise from for the dense tree obstruction, analogous to the dense urban obstructions in UMi.

That correlation in typical HSR scenarios is smaller than the correlation values in the cellular setting is worth emphasizing. In [12], we find the decorrelation distance in urban shadowing environments is smaller than the values in open environments (rural area), (e.g., $D = 44$ m at 1.6 km range and $D = 112$ m at 4.8 km range [6]). This also implies that the decorrelation distance is greater at longer link distances. In [17], the authors attributed this to the widths of the buildings and other obstructions that are close to the mobile, because the path profile changes most rapidly close to such obstructions as the mobile moves around them. In HSR measurements, the shadowing effect with respect to the distance dependent average path loss is mainly caused by the echoes from the large reflectors or scatterers and of course the actual obstructions (e.g., trees). The effect from scatterers is relatively small compared with that from the blocking objects. The standard deviation of these shadowing samples is relatively small, and the rapid train movement induces rapid phase changes and hence reduced correlation. In the blocked terrain, however, homogeneous large objects (trees in our measurement) obstruct the propagation paths between the transmitter and receiver for significant lengths of travel, yielding higher correlation. This phenomenon was also noted in [6].

5. Conclusion

A statistical analysis of shadowing propagation data obtained from measurements carried out in typical HSR environments was performed at 2350 MHz. Based on the reverse arrangement test method, the stationarity of shadowing data was validated. By means of the stationary property, we can set any geographical point between the transmitter and receiver as the starting position when conducting the shadowing evaluations, and we can use the experimental data from one measurement run for the channel parameterizations instead of large (and expensive-to-obtain) ensemble averages (statistical averages).

In some prior work, an independent log-normal random process was used for the shadowing characterization, but because of the nature of real-world propagation, we showed that the shadowing samples are indeed correlated. Three types of autocorrelation models were compared for describing the correlated shadowing propagation mechanisms. According to our NMSE results, it was found that the single exponential model offers the best fit for the three HSR environments, OV, TBV, and ORC, yielding decorrelation distances of 11.9 m, 17.7 m, and 8.3 m, respectively. The result of this work is useful for the evaluation and verification of wireless communications in HSR scenarios, which can be directly used in wireless coverage prediction.

Appendix

The WSS property can be verified by studying the variation in the series of correlated shadowing samples. Here we use the reverse arrangement test approach for the verification. This method does not require knowledge of the sampling distribution, and it involves the following: (a) computing the mean square values of samples in each subinterval; (b) performing the test of reverse arrangements. The main ideas are described in Validation Procedure [13].

Validation Procedure is as follows.

(1) Consider a sequence of N_s observations of a random variable λ, where the observations are denoted by λ_i, $i = 1, 2, 3, \ldots, N_s$. In the data analysis, the observation λ_i represents the value of the shadowing samples at the receiver.

(2) Define $\varepsilon_{ij} = \{1, \text{if } \lambda_i > \lambda_j; 0, \text{ otherwise}\}$.

(3) Count the total number of reverse arrangements $A = \sum_{i=1}^{N_s-1} A_i$, where $A_i = \sum_{j=i+1}^{N_s} \varepsilon_{ij}$. For example, $A_1 = \sum_{j=2}^{N_s} \varepsilon_{1j}$, $A_2 = \sum_{j=3}^{N_s} \varepsilon_{2j}$, and $A_3 = \sum_{j=4}^{N_s} \varepsilon_{3j}$.

(4) Calculate the acceptance region for the hypothesis. If the sequence of N_s observations is independent observations of the same random variable and for $N_s \geq 10$, the distribution for the number of reverse

arrangements is approximately a normal variable with a mean and a variance as follows [13, 18]: $\mu_A = N_s(N_s - 1)/4$, $\sigma_A^2 = N_s(N_s - 1)(2N_s + 5)/72$.

(5) Verify the stationarity hypothesis according to the acceptance region: $A_{N_s;(1-\alpha/2)} < A \leq A_{N_s;\alpha/2}$, where α is the desired level of significance for the test; usually $\alpha = 0.05$.

Now let it be hypothesized that the shadowing sample data are stationary. According to [13], we can get the acceptance region for this hypothesis for our data as $A_{20;1-0.05/2} = 64 \leq A \leq A_{20;0.025} = 125$. Note that when the amount of the intervals of N is less than or equal to 20, we can directly use the total number of reverse arrangements of A without the normalization. From Table A.6 in [13], for $\alpha = 0.05$, $A_{20;(1-\alpha/2)} = A_{20;1-0.05/2} = 64$ and $A_{20;\alpha/2} = A_{20;0.025} = 125$.

Competing Interests

The authors declare no competing interests.

Acknowledgments

The research was supported in part by the NSFC projects under Grant no. 61371070, Beijing Nova Programme (Grant no. xx2016023), Beijing Natural Science Foundation (Grant no. 4142041), and the open research fund of National Mobile Communications Research Laboratory, Southeast University (no. 2014D05).

References

[1] R. He, Z. Zhong, B. Ai, and J. Ding, "Propagation measurements and analysis for high-speed railway cutting scenario," *Electronics Letters*, vol. 47, no. 21, pp. 1167–1168, 2011.

[2] L. Liu, C. Tao, J. Qiu et al., "Position-based modeling for wireless channel on high-speed railway under a viaduct at 2.35 GHz," *IEEE Journal on Selected Areas in Communications*, vol. 30, no. 4, pp. 834–845, 2012.

[3] K. Guan, Z. Zhong, B. Ai, and T. Kurner, "Propagation measurements and analysis for train stations of high-speed railway at 930 MHz," *IEEE Transactions on Vehicular Technology*, vol. 63, no. 8, pp. 3499–3516, 2014.

[4] R. He, Z. Zhong, B. Ai, and C. Oestges, "Shadow fading correlation in high-speed railway environments," *IEEE Transactions on Vehicular Technology*, vol. 64, no. 7, pp. 2762–2772, 2015.

[5] B. Ai, X. Cheng, T. Kurner et al., "Challenges toward wireless communications for high-speed railway," *IEEE Transactions on Intelligent Transportation Systems*, vol. 15, no. 5, pp. 2143–2158, 2014.

[6] M. Gudmundson, "Correlation model for shadow fading in mobile radio systems," *Electronics Letters*, vol. 27, no. 23, pp. 2145–2146, 1991.

[7] F. Graziosi, M. Pratesi, M. Ruggieri, and F. Santucci, "A multicell model of handover initiation in mobile cellular networks," *IEEE Transactions on Vehicular Technology*, vol. 48, no. 3, pp. 802–814, 1999.

[8] F. Graziosi and F. Santucci, "A general correlation model for shadow fading in mobile radio systems," *IEEE Communications Letters*, vol. 6, no. 3, pp. 102–104, 2002.

[9] F. Luan, Y. Zhang, L. Xiao, C. Zhou, and S. Zhou, "Fading characteristics of wireless channel on high-speed railway in hilly terrain scenario," *International Journal of Antennas and Propagation*, vol. 2013, Article ID 378407, 9 pages, 2013.

[10] Y. Zhang, J. Zhang, D. Dongt, X. Nie, G. Liu, and P. Zhang, "A novel spatial autocorrelation model of shadow fading in urban macro environments," in *Proceedings of the IEEE Global Telecommunications Conference (GLOBECOM '08)*, pp. 4175–4179, New Orleans, La, USA, December 2008.

[11] L. Liu, C. Tao, T. Zhou, Y. Zhao, X. Yin, and H. Chen, "A highly efficient channel sounding method based on cellular communications for high-speed railway scenarios," *EURASIP Journal on Wireless Communications and Networking*, vol. 2012, article 307, pp. 1–16, 2012.

[12] ITU-R, "Guidelines for evaluation of radio transmission technologies for IMT-Advanced," Tech. Rep. ITU-R M.2135, 2008.

[13] J. S. Bendat and A. G. Piersol, *Random Data: Analysis and Measurement Procedures*, John Wiley & Sons, New York, NY, USA, 4th edition, 2010.

[14] N. B. Mandayam, P.-C. Chen, and J. M. Holtzman, "Minimum duration outage for cellular systems: a level crossing analysis," in *Proceedings of the IEEE 46th Vehicular Technology Conference Mobile Technology for the Human Race*, vol. 2, pp. 879–883, Atlanta, Ga, USA, May 1996.

[15] A. Mawira, "Models for the spatial correlation functions of the (log)-normal component of the variability of VHF/UHF field strength in urban environment," in *Proceedings of the 3rd IEEE International Symposium on Personal, Indoor and Mobile Radio Communications (PIMRC '92)*, pp. 436–440, Boston, Mass, USA, October 1992.

[16] P. Taaghol and R. Tafazolli, "Correlation model for shadow fading in land-mobile satellite systems," *Electronics Letters*, vol. 33, no. 15, pp. 1287–1289, 1997.

[17] S. R. Saunders and A. Aragon-Zavala, *Antennas and Propagation for Wireless Communication Systems*, John Wiley & Sons, New York, NY, USA, 2007.

[18] S. B. Julius, L. D. Enochson, and A. G. Piersol, "Tests for randomness, stationary, normality and comparison of spectra," Tech. Rep., Air Force Flight Dynamics Laboratory, 1965.